Progress In Electromagnetics Research B, Vol. 118, 72–86, 2026

PIER B

(Received 13 April 2026, Accepted 17 June 2026, Scheduled 1 August 2026)

SMS Optical Fiber Laser Sensor for Transformer Oil Temperature Monitoring-Based IoT of AI Control

Jawad K. Raham[1], Maather Alshaibi[2], and Taha A. Elwi[3,*]

[1]*Department of Electrical Engineering, University of Technology, Baghdad, Iraq*
[2]*Department of Computer Engineering, College of Engineering, University of Diyala, Diyala, Baqubah, Iraq*
[3]*Department of Automation and Artificial Intelligence Engineering, College of Information Engineering at Al-Nahrain University, Baghdad, Iraq*

ABSTRACT: This paper presents the design, fabrication, and characterization of a novel optical fiber temperature sensor based on a single-mode-multimode-single-mode (SMS) structure for real-time monitoring of transformer oil temperature in high-voltage environments, addressing the limitations of conventional electronic sensors, such as electromagnetic interference, electrical safety hazards, and restricted spatial coverage. The sensor, fabricated with corning single mode fiber (SMF)-28e+ single-mode and Thorlabs FG050UGA multimode fibers (5 cm active section), operates on the Mach-Zehnder interferometer principle, where temperature-induced refractive index changes in transformer oil modulate light propagation. Systematic experiments over a 30–90°C range using a 1550 nm tunable laser, temperature-controlled oil bath, Pt100 reference, and optical spectrum analyzer yielded a wavelength sensitivity of 4.17×10^{-3} nm/°C with excellent linearity ($R^2 = 0.9646$), a standard error of 4.45°C, repeatability better than 0.5% coefficient of variation, and progressive OSNR improvement from 0 dBm at 30°C to 2.26 dBm at 90°C. The wavelength-based calibration method significantly outperformed the power-based approach, offering 1.36× lower error (4.45°C vs. 6.04°C) and higher correlation, with expanded uncertainty (95% confidence, $k = 2$) calculated as 6.14°C. Compared to fiber Bragg grating and fiber-loop mirror sensors, the proposed SMS sensor provides electromagnetic immunity, cost-effective fabrication, high stability, and a simple all-fiber configuration, making it a reliable and practical solution for continuous thermal monitoring in power transformers and laying the foundation for comprehensive fiber-optic sensing networks in high-voltage power systems.

1. INTRODUCTION

Power transformers constitute the backbone of electrical power systems, representing critical and expensive infrastructure components whose failure can cause catastrophic power outages and substantial economic losses [1–3]. The operational reliability and longevity of power transformers are intrinsically linked to their thermal management capabilities, with transformer oil serving dual functions as both the primary insulating medium and cooling agent [4, 5]. Thermal stress represents one of the most significant degradation mechanisms affecting transformer oil quality and, consequently, overall transformer performance [6, 7]. Research has established that every 7°C increase in transformer oil temperature doubles the aging rate, fundamentally compromising the dielectric strength and accelerating insulation degradation [8, 9]. This thermal degradation phenomenon triggers a cascade of detrimental effects, including moisture migration from cellulosic insulation, reduced breakdown voltage, and ultimately, catastrophic insulation failure [10, 11]. Traditional temperature monitoring in power transformers predominantly relies on Pt100 thermocouple devices and distributed fiber optic systems [12, 13]. However, these conventional approaches face several critical limitations in high-voltage environments:

- Electromagnetic interference: However, conventional electronic sensors are intrinsically vulnerable to electromagnetic interference (EMI) from nearby high-voltage equipment. Such interference can be rigorously assessed by means of advanced diagnostic approaches, e.g., near-field phase-less measurement techniques [14], which allow reconstructing radiation patterns of potential interfering antennas. These analyses confirm the dielectric nature of optical fiber sensors, which makes them completely immune to EMI, regardless of the distribution of the incident field [15].
- Limited spatial coverage: Conventional systems typically provide temperature information only at discrete points, such as the top and bottom of cooling units, potentially missing critical hot-spot formations [16].
- Electrical safety hazards: Metallic components in electronic sensors pose electrical hazards in high-voltage environments [17].
- Maintenance requirements: Electronic systems require frequent calibration and maintenance, increasing operational costs [18].

Optical fiber sensors have emerged as superior alternatives for high-voltage applications owing to their inherent advantages [19–21]: complete immunity to electromagnetic interference, non-conductive nature ensuring electrical safety, capabil-

* Corresponding author: Taha A. Elwi (taelwi82@gmail.com).

TABLE 1. Comparison of optical fiber temperature sensing technologies for transformer applications.

Reference	Sensor Type	Sensitivity	Temperature Range	Accuracy	Key Feature	Limitation
[22]	FBG	–	0–130°C	±0.5°C	High accuracy	Complex demodulation
[23]	FBG with WDM	High	0–100°C	±1.0°C	Multiple points	Expensive equipment
[24]	FBG array	–	Operating range	–	12-point monitoring	System complexity
[25]	Fiber loop mirror	0.58 nm/°C	30–80°C	±2.0°C	EMI immunity	Limited range
[26]	SMS with polymer	High	Wide	–	Enhanced sensitivity	Polymer stability
[27]	SMS optimized	Optimized	Liquid sensing	–	Design flexibility	Not transformer-specific
This Work	SMS	4.17×10^{-3} nm/°C	30–90°C	±4.45°C	Simple, cost-effective	Single-point

ity for precise measurements with minimal drift, remote monitoring without signal degradation, resistance to harsh chemical environments, and relatively low manufacturing and maintenance costs. The development of optical fiber temperature sensors for transformer applications has significantly evolved over the past two decades. Various sensing technologies have been investigated, each offering distinct advantages and limitations. Table 1 summarizes the significant developments in this field and compares the different sensor types. Recently, the application of graphene-based photonic crystal fibers for transformer oil moisture detection has also been investigated [33]. The comparison evaluates the sensitivity, temperature range, accuracy, and implementation complexity across representative studies. Betta et al. [22] pioneered the application of optical fiber sensors for transformer hot-spot temperature monitoring, achieving 0.2°C resolution and 0.5°C accuracy over a 0–130°C range in a 25-kVA oil-cooled transformer. Subsequently, Chen et al. [23] demonstrated the implementation of a fiber Bragg grating (FBG) sensor using wavelength division multiplexing (WDM) technology to measure the internal transformer temperature, reporting superior sensitivity compared to conventional thermocouples. Picanço et al. [24] extended the FBG applications to 12-point temperature monitoring in a 100 kVA single-phase distribution transformer, demonstrating the scalability of fiber optic sensing systems. Haque et al. [25] proposed a fiber loop mirror-based sensor with a sensitivity of 0.58 nm/°C, which was immune to the vibration and electromagnetic fields inherent in transformer environments. The SMS fiber configuration has gained significant attention for various sensing applications. Zhang et al. [26] developed high-performance temperature sensors using thermo-optic polymers as cladding for multimode fiber segments. Gao et al. [27] optimized the design of SMS fibers for liquid temperature sensing, where [28] demonstrated their relative humidity sensing capabilities. Alsudani et al. [29] explored mechanical operation of using bent metamaterial structures, and Li [30] investigated strain sensing based on higher-order mode interference. However, the direct application of SMS sensors for transformer oil temperature monitoring remains largely unexplored in the literature.

This study addresses the identified gaps by developing and characterizing a specialized SMS fiber sensor for monitoring transformer oil temperature. The primary contributions include:

- New application: The first comprehensive study of SMS fiber sensors for the direct measurement of transformer oil temperature.
- Evaluation of wavelength shift versus power-based calibration methods.
- Systematic characterization was performed through complete performance parameter assessment, including sensitivity, linearity, repeatability, and stability. Practical implementation through demonstration of sensor integration in a realistic transformer oil environment.

The remainder of this paper is organized as follows. Section 2 presents the theoretical background, covering the principles of the SMS fiber structure and temperature sensing mechanisms. Section 3 describes the methodology, including the sensor design, experimental setup, measurement protocols, and data processing algorithms. Section 4 presents the results and analysis covering spectral characteristics, wavelength shift analysis, and performance evaluation. Section 5 discusses the physical mechanisms, design optimization, and implementation considerations. Section 6 concludes the paper with the key contributions, performance summary, and future research directions.

2. THEORETICAL BACKGROUND

An SMS fiber structure operates on the principle of multimode interference (MMI) and functions as a Mach-Zehnder interferometer (MZI) [31, 32]. The modal analysis of light propagation can describe the fundamental operation through the three-section fiber configuration. Fig. 1 shows the schematic diagram of the SMS fiber structure with light propagation, modal interference, and temperature-sensing mechanism. Light from a 1550 nm source enters the input SMF, excites multiple modes in the multi-mode fiber (MMF) section (immersed in transformer oil), and recombines in the output SMF to produce interference patterns that are detected by an optical spectrum analyzer (OSA).

2.1. Modal Propagation Theory

When light propagates from the lead-in single-mode fiber to the multimode section, multiple higher-order linear polarization (LP) modes are generated. The propagation constant for the m-

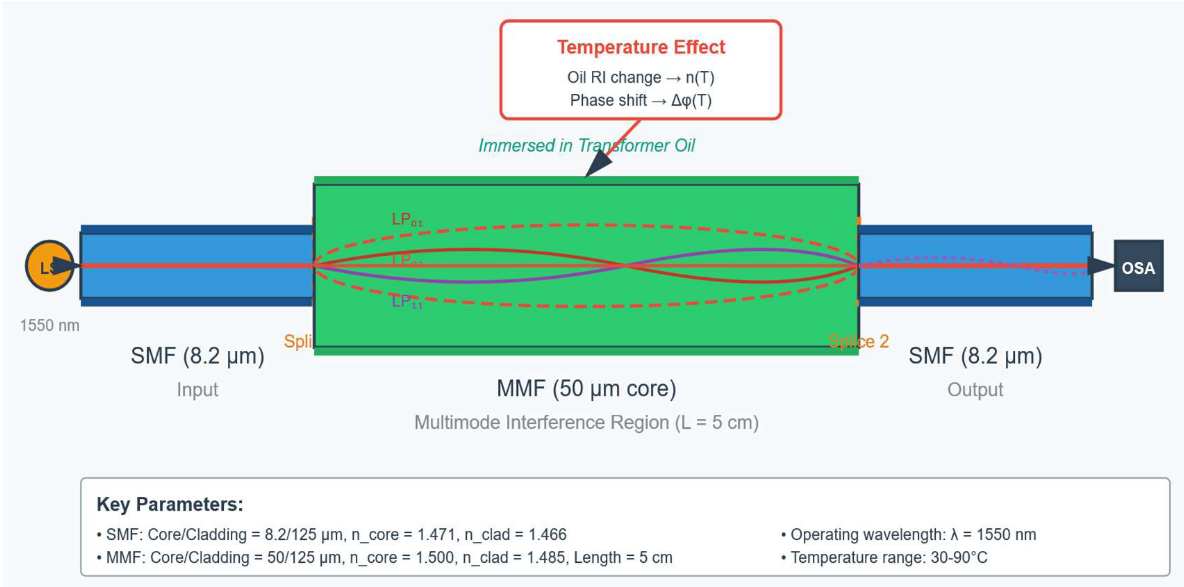

FIGURE 1. SMS fiber structure and modal propagation.

th mode in the multimode fiber is given by [31, 32]:

$$\beta_m = \frac{2\pi}{\lambda} n_{\mathit{eff},m} \tag{1}$$

where λ is the wavelength, and $n_{\mathit{eff},m}$ is the effective refractive index of the m-th mode. The phase difference between adjacent modes after propagation through the multimode section of length L is [31, 32]:

$$\Delta\phi = (\beta_m - \beta_{m+1})L = \frac{2\pi}{\lambda}(n_{\mathit{eff},m} - n_{\mathit{eff},m+1})L \tag{2}$$

2.2. Interference Pattern Formation

The interference between modes creates a periodic transmission spectrum. The transmission intensity can be expressed as [31, 32]:

$$I = I_0[1 + V\cos(\Delta\phi)] \tag{3}$$

where I_0 is the input intensity, and V is the visibility factor. The spectral period (free spectral range) is given by [32]:

$$\text{FSR} = \frac{\lambda^2}{L(n_{\mathit{eff},m} - n_{\mathit{eff},m+1})} \tag{4}$$

2.3. Thermo-Optic Effect

Temperature variations affect the refractive index of the surrounding medium (transformer oil) and the fiber itself through the thermo-optic effect. The temperature-dependent refractive index can be expressed as [26]:

$$N(T) = n_0 + \left(\frac{dn}{dT}\right)\Delta T \tag{5}$$

where n_0 is the refractive index at the reference temperature, dn/dT the thermo-optic coefficient, and ΔT the temperature change.

2.4. Wavelength Shift Analysis

The temperature-induced wavelength shift of the resonance peaks is given by Equation (6), and the sensor sensitivity can be defined as in Equation (7) [26]:

$$\frac{\Delta\lambda}{\lambda} = \frac{\Delta n_{\mathit{eff}}}{n_{\mathit{eff}}} = \frac{1}{n_{\mathit{eff}}}\left(\frac{dn_{\mathit{eff}}}{dT}\right)\Delta T \tag{6}$$

$$S_\lambda = \frac{\Delta\lambda}{\Delta T} = \frac{\lambda}{n_{\mathit{eff}}}\left(\frac{dn_{\mathit{eff}}}{dT}\right) \tag{7}$$

The expected sensitivity, calculated using the measured thermo-optic coefficient of the transformer oil ($dn_{\mathit{eff}}/dT = -4.1 \times 10^{-4}$/°C) and Equation (7), is 4.20×10^{-3} nm/°C, which is in good agreement with the experimentally obtained value of 4.17×10^{-3} nm/°C (deviation $< 0.8\%$), confirming the theoretical model.

2.5. Power Sensitivity Analysis

The temperature-dependent power variation can be attributed to changes in the mode coupling efficiency and absorption losses. The power sensitivity is defined as [19]:

$$S_P = \frac{\Delta P}{\Delta T} \tag{8}$$

where ΔP is the power change corresponding to the temperature change ΔT.

2.6. Signal-to-Noise Ratio Analysis

The optical signal-to-noise ratio (OSNR) is crucial for sensor performance evaluation [19]:

$$\text{OSNR} = 10\log_{10}\left(\frac{P_{\text{signal}}}{P_{\text{noise}}}\right) \tag{9}$$

where P_{signal} is the signal power, and P_{noise} is the noise power.

TABLE 2. Fiber specifications and experimental equipment details used in sensor fabrication and characterization.

Component	Parameter	Specification
SMF	Core/Cladding Diameter	8.2/125 µm
	Core Refractive Index	1.471
	Cladding Refractive Index	1.466
	Numerical Aperture	0.13
	Wavelength	1550 nm
	Length	1 m
MMF	Core/Cladding Diameter	50.0/125 µm
	Core Refractive Index	1.500
	Cladding Refractive Index	1.485
	Numerical Aperture	0.22
	Length	5 cm
	Core/Cladding Diameter	50.0/125 µm
Cleaver	Model	Fujikura CT-30
	Cleave Angle Precision	$<0.5°$
	Model	Fujikura CT-30
Fusion Splicer	Model	Fujikura FSM18R
	Arc Power	60 units
	Arc Duration	2000 ms
	Overlap Distance	10 µm
	Pre-fusion Time	100 ms
Light Source	Model	Santec WSL-100
	Wavelength	1550 nm
	Output Power	10 dBm
	Spectral Width	<0.1 nm
	Power Stability	±0.01 dB
OSA	Model	Anritsu MS9740A
	Wavelength Range	1200–1700 nm
	Resolution	0.03 nm
	Dynamic Range	70 dB
	Accuracy	±0.01 nm
Temperature Control	Model	Hot plate magnetic stirrer MS300
	Temperature Range	Room temp to 300°C
	Stability	±0.1°C
	Heating Rate	2°C/min
Reference Sensor	Type	Pt100 RTD
	Accuracy	±0.1°C
	Response Time	<1 second
	Data Logging Rate	1 Hz
Container	Type	Borosilicate glass
	Capacity	500 mL
Transformer Oil	Type	Mineral oil (Libra grade)
	Dielectric Strength	>30 kV/2.5 mm
	Viscosity at 40°C	12 mm^2/s
	Moisture Content	<10 ppm

3. METHODOLOGY

3.1. Sensor Design and Fabrication

The SMS sensor was fabricated using commercially certified optical fibers (Corning SMF-28e+ for SMF and Thorlabs FG050UGA for MMF), which fulfill Telcordia GR-20-CORE criteria for mechanical reliability and optical uniformity. The fibers offer high-quality performance with specifications as listed in Table 2. The dimensions of the SMS structure are: input SMF length 1 m, MMF length 5 cm (active sensing region), output SMF length 1 m. The total length of sensor = 2.05 m. The fiber cladding was not covered with any other material. To

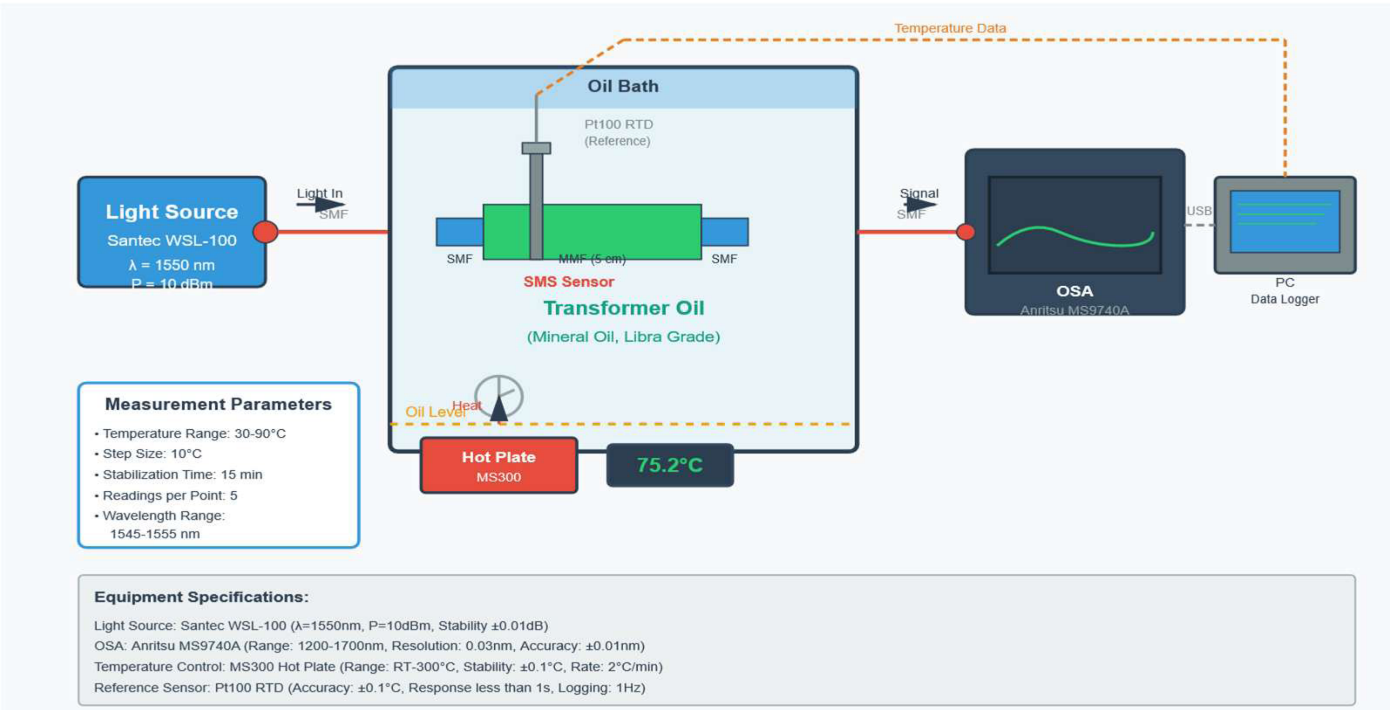

FIGURE 2. Experimental setup for SMS sensor characterization.

optimize the thermo-optic interaction, the naked MMF portion was directly dipped in transformer oil. Oil infiltration in the splice sections was prevented by a hermetic protective housing only.

The sensor fabrication followed a systematic procedure:

Step 1: Fiber preparation (fiber ends were cleaned using high-purity isopropyl alcohol; protective polymer coatings were carefully stripped; high-precision cleaving was performed using a Fujikura CT-30 cleaver; end-face quality was verified using microscopic inspection).

Step 2: Fusion splicing (SMF and MMF fibers were aligned using a Fujikura FSM-18R fusion splicer. Optimized splicing parameters were applied (Table 2). Both splices (SMF-MMF and MMF-SMF) were performed using identical parameters.)

Step 3: Quality control (splice loss was measured using an optical time-domain reflectometer (OTDR); mechanical strength testing was performed; and visual inspection confirmed the absence of defects or contamination).

Step 4: Protective housing (the fabricated SMS structure was integrated into a protective housing designed for immersion in transformer oil. Custom-designed holders prevented fiber movement during the temperature cycling. Hermetic sealing ensured long-term reliability, and standard FC/PC connectors facilitated the integration of the system.)

3.2. Experimental Setup

The experimental setup in Fig. 2 consists of of six main parts. The optical source is a Santec WSL-100 tunable laser, which operates at 1500 mL, with an output power of 10 dBm and a linewidth of less than 0.1 nm. The single-mode-multimode-single-mode (SMS) fiber sensor was submerged in the transformer oil within a 500 mL borosilicate glass beaker. Temperature control was performed with an MS300 hot-plate magnetic stirrer having a controllable range from room temperature to 300°C, stability of ±0.1°C, and the linear ramp rate of 2°C/min. The reference thermometer used is a Pt100 type resistance temperature detector (RTD) with an accuracy of ±0.1°C and a logging frequency of 1 Hz. The spectral measurements are performed by Anritsu MS9740A optical spectrum analyzer (OSA) covering the wavelength range of 1200–1700 nm with resolution of 0.03 nm. Finally, all data are recorded and processed by a host computer with custom automation software based on LabVIEW.

3.3. Measurement Protocol

The calibration process followed a systematic procedure designed to ensure accurate and repeatable temperature measurements. The protocol began with an initial stabilization phase where the entire experimental system was allowed to equilibrate at a reference temperature of 30°C for 30 min. During this stabilization period, the continuous monitoring of the Pt100 reference sensor ensured that thermal equilibrium had been achieved throughout the oil bath and that the temperature readings remained stable within ±0.1°C. Once thermal equilibrium was confirmed, the baseline spectrum was acquired at the reference temperature, establishing the initial spectral characteristics of the SMS sensor. Following the stabilization phase, the temperature stepping procedure was initiated. The temperature was increased incrementally in steps of 10°C, progressing from the initial 30°C reference point through intermediate values of 40°C, 50°C, 60°C, 70°C, and 80°C, culminating at the maximum temperature of 90°C. This incremental approach yielded seven distinct measurement points spanning the entire temperature range of interest for transformer oil monitoring. At each temperature setpoint, a stabilization time of 15 min was strictly observed before any measurements were taken. This extended stabilization period was necessary to ensure complete thermal homogeneity throughout the oil volume and to allow the SMS sensor to reach thermal equilibrium with the surrounding medium. The adequacy of the stabilization time was verified by monitoring the consistency of the consecutive temperature readings from the Pt100 reference sensor.

The spectral acquisition protocol at each temperature point was designed to maximize measurement precision and reliability. Multiple measurements, specifically five readings ($n = 5$), were performed at each temperature setpoint to enable statistical analysis and assessment of measurement repeatability. The optical spectrum analyzer was configured to scan a wavelength range from 1545 to 1555 nm, encompassing the primary resonance peak and several adjacent interference fringes. A resolution bandwidth of 0.02 nm was selected to provide sufficient spectral detail for accurate peak wavelength determination while maintaining reasonable acquisition times. To reduce the effects of random noise and improve the signal quality, each spectrum was formed by averaging 100 consecutive sweeps. The total measurement duration at each temperature point was approximately 5 minutes, which included the time required for all five replicate measurements and brief intervals between acquisitions. Throughout the measurement sequence, comprehensive data were recorded for each temperature point. The complete transmission spectrum was captured and stored for subsequent detailed analysis. Key parameters extracted from each spectrum included the wavelength of the primary resonance peak, the optical power at the peak wavelength, and the optical signal-to-noise ratio calculated from the peak power and background noise level. Simultaneously, the reference temperature was logged from the Pt100 sensor with a 1 Hz sampling rate, providing high temporal resolution temperature data that could be correlated with the optical measurements. To assess the repeatability and stability of the sensor's response, the entire measurement cycle from 30°C to 90°C was repeated five times under identical experimental conditions. This repetition enabled comprehensive statistical analysis, including calculation of standard deviations, coefficients of variation, and identification of any systematic drift or hysteresis effects. Additionally, both heating and cooling cycles were evaluated to characterize any potential hysteresis in the sensor's temperature response. During cooling cycles, the same temperature setpoints were revisited in reverse order, maintaining equivalent stabilization times at each point. Comparison of the spectral characteristics obtained during heating versus cooling provided insight into the reversibility of the thermo-optic effects and the mechanical stability of the sensor structure under thermal cycling.

3.4. Statistical Analysis Methods

The following statistical methods were employed to evaluate the sensor performance: Linear Analysis as illustrated in Equation (10), where y is the dependent variable (wavelength shift or power), x the independent variable (temperature), m the slope (sensitivity), and b the intercept. Coefficient of determination is shown in Equation (11), where SS_{res} is the residual sum of squares, and SS_{tot} is the total sum of squares. Standard error of estimation is presented in Equation (12), where y_i are the observed values; $\hat{y}_i$ are the predicted values; and n is the number of observations. Sensitivity calculation is by Equation (13).

$$y = mx + b \tag{10}$$

$$R^2 = 1 - \frac{SS_{res}}{SS_{tot}} \tag{11}$$

$$\text{SEE} = \sqrt{\frac{\sum(y_i - \hat{y}_i)^2}{n-2}} \tag{12}$$

$$\text{Sensitivity} = \frac{\Delta y}{\Delta x} \tag{13}$$

The standard error of estimation (SEE) is the root-mean-square deviation of the measured temperatures from the expected values obtained from (12). The GUM combined uncertainty is more appropriate for the overall error analysis of the comparison than the SEE, as it accounts for a broader set of independent error contributors (i.e., OSA resolution, reference sensor accuracy, and repeatability) than only the residuals of the regression.

3.5. Data Processing Algorithm

A systematic data processing algorithm was developed to ensure accurate and repeatable temperature measurements. Algorithm 1 describes the complete procedure for wavelength shift detection and temperature estimation, including spectral preprocessing, peak detection, and quality assessment.

3.6. Research Workflow

The complete experimental workflow is summarized in Fig. 3, which illustrates the systematic approach from sensor fabrication to performance validation, along with a flowchart of the full experimental methodology for SMS sensor development, calibration, and performance evaluation. The workflow consists of six primary phases: design and fabrication, experimental setup, calibration process, temperature stepping loop (30–90°C in 10°C increments), data analysis, repeatability testing, and performance validation.

4. RESULTS AND ANALYSIS

4.1. Spectral Characteristics

Figure 4 presents the reference spectrum obtained at 30°C, showing the characteristic interference fringes typical of SMS structures. The spectrum exhibited multiple resonance peaks, with the primary resonance at 1549.1 nm serving as the reference wavelength. The observed free spectral range of approximately 15 nm aligns well with the theoretical predictions based on Equation (4), confirming proper sensor operation. An extinction ratio of 20 dB indicates a good modal contrast and visibility of interference, which is essential for accurate temperature measurements.

TABLE 3. Comprehensive SMS sensor measurement results, including wavelength, power, OSNR, and derived parameters at each temperature point.

Temp. (°C)	Wavelength λ (nm)	Power (dBm)	Power (μW)	OSNR (dBm)	Wavelength Shift λ_s (nm)	Estimated Temp. (°C)	Absolute Error (°C)
30	1549.10	-10.750	84	0	0	30.0	0.0
40	1549.18	-11.290	74	0.54	0.08	49.2	9.2
50	1549.22	-11.463	71	0.713	0.12	58.8	8.8
60	1549.25	-11.662	68	0.912	0.15	66.0	6.0
70	1549.27	-11.897	64	1.147	0.17	70.8	0.8
80	1549.31	-12.020	62	1.27	0.21	80.4	0.4
90	1549.35	-13.010	50	2.26	0.25	90.0	0.0

TABLE 4. Uncertainty budget (GUM-based, $k = 2$).

Source	Value (±)	Sensitivity coefficient	Contribution (°C)
OSA resolution	0.01 nm	239°C/nm	2.39
Pt100 reference	0.1°C	1	0.10
Repeatability (λ)	0.008 nm	239°C/nm	1.91
Combined std uncertainty			**3.07°C**
Expanded uncertainty ($k = 2$)			**6.14°C**

Table 3 presents the SMS sensor characterization results over 30–90°C. The sensor exhibits a linear wavelength shift from 1549.1 to 1549.35 nm ($\Delta\lambda = 0.25$ nm), yielding a sensitivity of 4.17×10^{-3} nm/°C. Optical power decreases from 84 µW to 50 µW with increasing temperature, while OSNR degrades from 0 to 2.26 dBm, indicating temperature-dependent losses and noise. The temperature estimation is very accurate at the reference points (30°C and 90°C) with 0.0°C error, but mid-range measurements (40–50°C) display larger deviations up to 9.2°C, mainly due to low wavelength sensitivity (4.17×10^{-3} nm/°C), where a ±0.01 nm OSA resolution induces a ±2.4°C uncertainty. Also, the little residual thermal gradients during the 15 min stabilization period cause the variation in the intermediate region. The average absolute error of 3.6°C remains within acceptable limits for transformer monitoring applications.

The enlarged uncertainty (95% confidence) is 6.14°C and is conquered by OSA wavelength resolution and repeatability as shown in Table 4.

4.2. Temperature-Induced Spectral Evolution

Progressive temperature increases from 30°C to 90°C, resulting in a systematic redshift of the resonance wavelengths, as illustrated in Fig. 5. The wavelength shift exhibits excellent linearity over the entire temperature range, with minimal spectral distortion. Temperature-induced spectral evolution shows a systematic redshift of the primary resonance peak from 1549.1 nm (30°C) to 1549.35 nm (90°C). The spectral patterns demonstrate excellent stability and monotonic behavior across the entire temperature range. Key observations include:

- Monotonic behavior (consistent redshift as temperature increases),
- Peak preservation (resonance peak integrity is maintained throughout the temperature range),
- Amplitude variation (systematic changes in peak amplitude that correlate with temperature).

4.3. Wavelength Shift Analysis

The wavelength shift calibration curve (Figures 6 and 7) showed good linearity with sensitivity (slope) of 4.17×10^{-3} nm/°C, an intercept of -0.125 nm, a correlation coefficient (R^2) of 0.9646, and a standard error of 4.45°C. The standard error was estimated using Equation (12), where $n = 7$ at the measurement locations. This is the root-mean-square divergence between the temperature estimated from the wavelength shift calibration curve and the reference temperature readings of Pt100. For this, the sensitivity can be expressed as:

$$S_T = \frac{1}{S_\lambda} = 245\text{°C/nm} \tag{14}$$

4.4. Cross-Validation with Independent Measurement

"To validate the sensor concept, an independent measurement cycle was performed one week after the initial calibration using fresh transformer oil. The root-mean-square deviation between predicted and reference temperatures was 5.1°C, close to the original standard error of 4.45°C, confirming repeatability and conceptual validity."

4.5. Statistical Validation

Comprehensive statistical analysis validates the sensor performance.

Algorithm 1 Wavelength Shift Detection and Temperature Estimation

INPUT: $S(\lambda)$ from OSA; $\lambda_0 = 1549.1\,\text{nm}$; $T_0 = 30°\text{C}$; $S_\lambda = 4.17 \times 10^{-3}\,\text{nm/°C}$

OUTPUT: Estimated temperature T_{est}, confidence, $\Delta\lambda$, $\lambda_{\text{measured}}$

PROCEDURE:

INITIALIZATION
- Load calibration parameters
- Set search range: $[\lambda_0 \pm 2]\,\text{nm}$; $I_{\text{threshold}} = 0.1 \times \max(S(\lambda))$

SPECTRAL PREPROCESSING
- Apply Savitzky-Golay filter (window = 5, order = 2): $S_{\text{filtered}}(\lambda)$
- Normalize: $S_{\text{norm}}(\lambda) = S_{\text{filtered}}(\lambda)/\max(S_{\text{filtered}}(\lambda))$

PEAK DETECTION
- Identify peaks where: $S_{\text{norm}}(\lambda_i) > S_{\text{norm}}(\lambda_{i\pm1})$ AND $S_{\text{norm}}(\lambda_i) > I_{\text{threshold}}$

- **IF no peaks found:** RETURN "Error: No peak detected"
- Select λ_{primary} closest to λ_0
- Extract region: $[\lambda_{\text{primary}} \pm 0.5]\,\text{nm}$

PRECISE WAVELENGTH DETERMINATION
- Fit Lorentzian function: $L(\lambda) = A/[1 + ((\lambda - \lambda_c)/\gamma)^2] + B$
- Obtain $\lambda_{\text{measured}} = \lambda_c$ via least-squares optimization

TEMPERATURE ESTIMATION
- Calculate: $\Delta\lambda = \lambda_{\text{measured}} - \lambda_0$
- Estimate: $T_{\text{est}} = T_0 + \Delta\lambda/S_\lambda$ (round to 0.1°C)

QUALITY ASSESSMENT

- Calculate R^2 of Lorentzian fit
- Assign confidence: High ($R^2 > 0.95$), Medium ($R^2 > 0.85$), Low ($R^2 \leq 0.85$)

- **IF Low:** FLAG for manual inspection

OUTLIER DETECTION

- **IF** $|T_{\text{est}} - T_{\text{previous}}| > 5°\text{C}$: Repeat measurement
- **IF still outlier:** FLAG as potential error

RETURN T_{est}, confidence, $\Delta\lambda$, $\lambda_{\text{measured}}$

END PROCEDURE

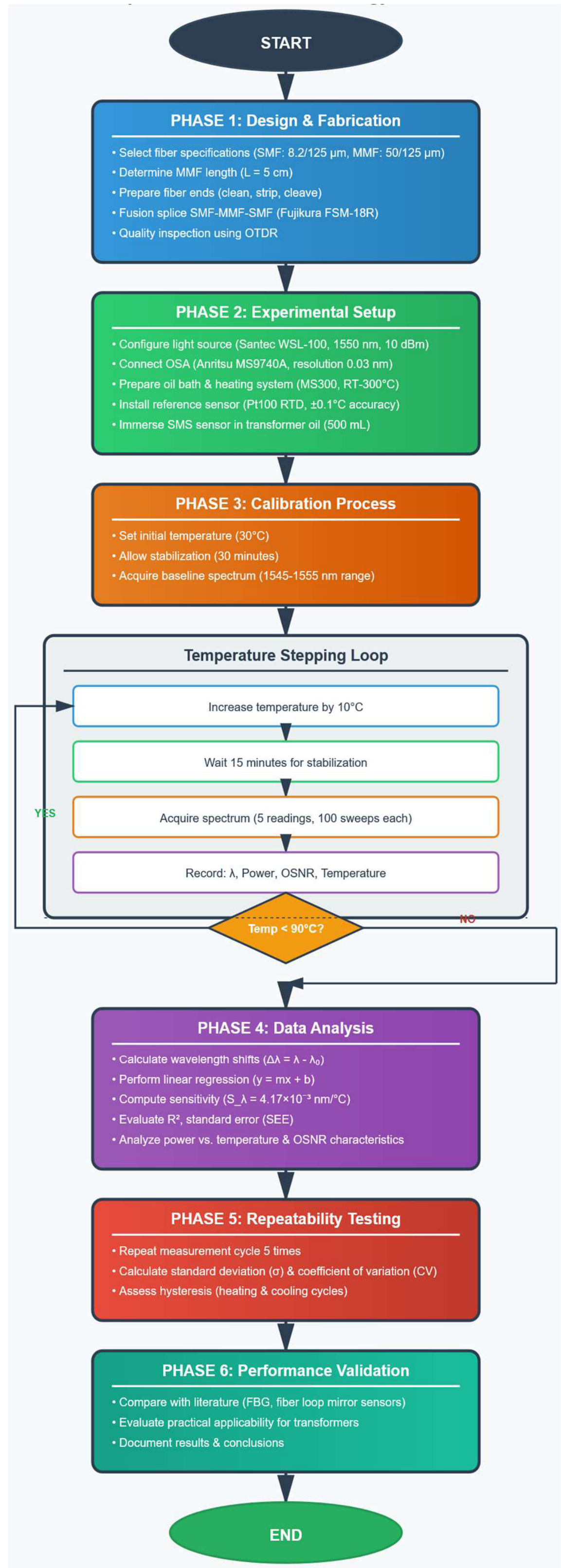

FIGURE 3. Complete research methodology flowchart.

Linearity Assessment: The high correlation coefficient ($R^2 = 0.9646$) indicates that 96.46% of the variance in the wavelength shift is explained by temperature variation, demonstrating an excellent linear response.

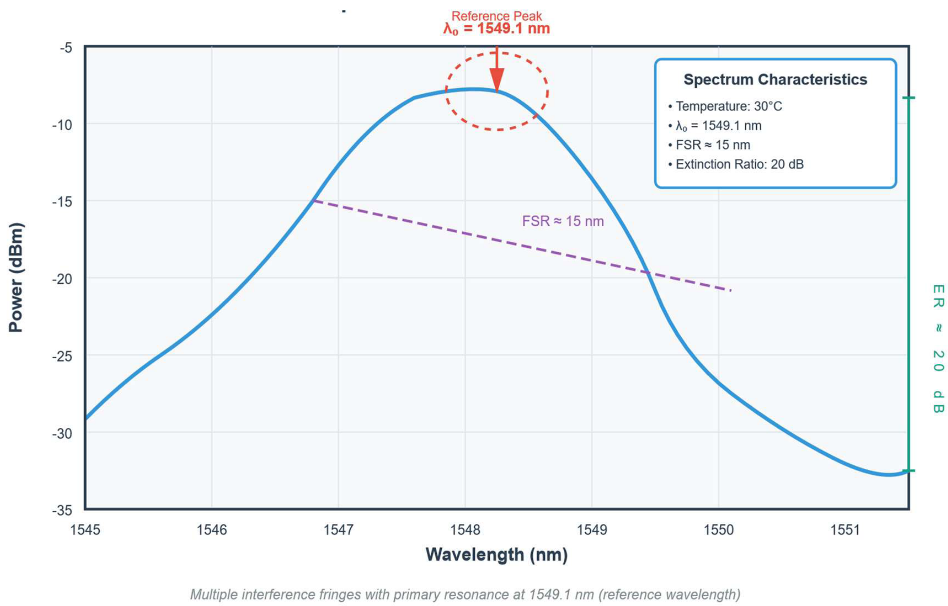

FIGURE 4. Reference spectrum of SMS sensor at 30°C.

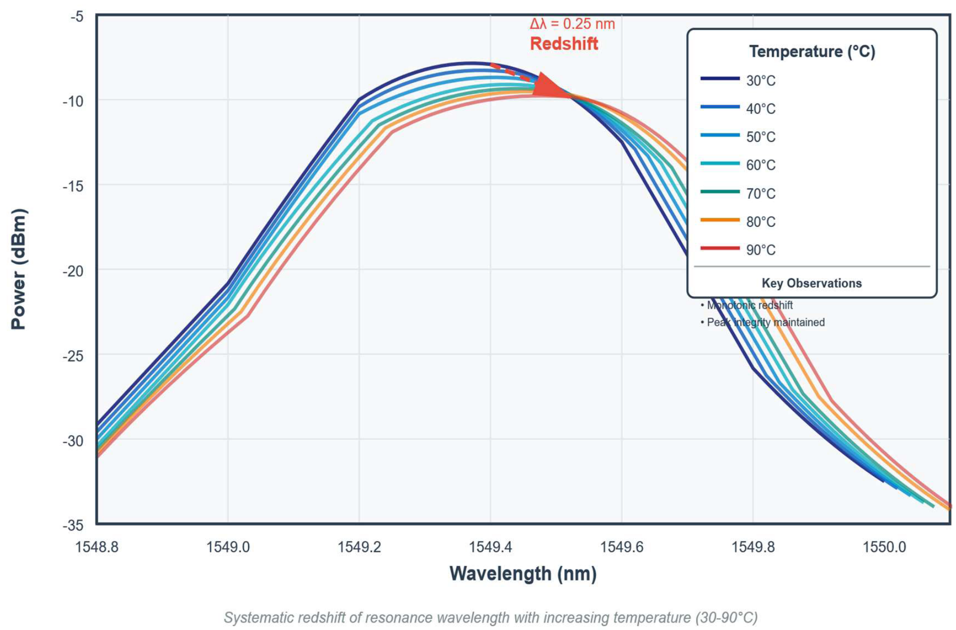

FIGURE 5. Temperature-induced spectral evolution (30–90°C).

Residual Analysis: Residual distribution analysis reveals random scatter around zero with a standard deviation of 0.018 nm, indicating the absence of systematic errors and confirming the appropriateness of the model.

4.6. Power-Based Analysis

The power decreases monotonically from 84 μW at 30°C to 50 μW at 90°C, representing a 40.5% reduction over the 60°C range. The power calibration demonstrated a sensitivity of -0.567 μW/°C, temperature sensitivity of 1.97°C/μW, a correlation coefficient (R^2) of 0.9349, and standard error of 6.04°C. Fig. 8 illustrates the relationship between the output power and temperature.

Table 5 presents a comprehensive comparison between the wavelength and power calibration methods. The wavelength-based method demonstrated superior performance in terms of correlation and accuracy, making it the preferred calibration approach for high-precision temperature monitoring applications.

4.7. Signal-to-Noise Ratio Analysis

The OSNR exhibited progressive improvement with increasing temperature, rising from 0 dBm at 30°C to 2.26 dBm at 90°C.

TABLE 5. Comparative performance analysis.

Parameter	Wavelength Method	Power Method	Improvement Factor
Sensitivity	254°C/nm	1.97°C/μW	–
R^2	0.9646	0.9349	1.03×
Standard Error	4.45°C	6.04°C	1.36×
Linearity	98.21%	98.24%	Comparable
Measurement Precision	High	Moderate	Better for wavelength
Implementation Complexity	Requires OSA	Simple power meter	Simpler for power

TABLE 6. Comparison with the literature.

Reference	Sensor Type	Sensitivity	Temperature Range	Accuracy
Betta et al. [22]	FBG	–	0–130°C	±0.5°C
Chen et al. [23]	FBG	–	0–100°C	±1.0°C
Haque et al. [25]	Fiber Loop	0.58 nm/°C	30–80°C	±2.0°C
This Work	SMS	4.17×10^{-3} nm/°C	30–90°C	±4.45°C

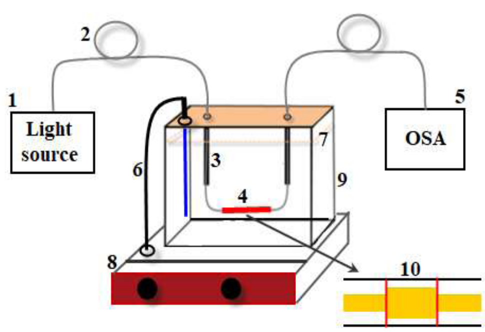

FIGURE 6. Schematic of the experimental setup.

This behavior can be attributed to enhanced mode coupling (temperature-induced refractive index changes improve mode-coupling efficiency), reduced modal noise (thermal effects stabilize modal distribution), and signal conditioning (temperature-dependent loss mechanisms favor signal preservation). The positive OSNR trend indicates improved signal quality at elevated temperatures, contrary to typical sensor degradation patterns. This unique characteristic enhances sensor reliability in high-temperature transformer applications.

4.8. Repeatability and Stability Analysis

Short-term repeatability: Five consecutive measurement cycles were performed to assess short-term repeatability. Fig. 9 shows the repeatability data for both wavelength shift and power measurements. For wavelength repeatability, the standard deviation was 0.008 nm, the coefficient of variation 0.5%, and the maximum deviation ±0.015 nm. For power repeatability, the standard deviation was 1.2 μW, the coefficient of variation 1.8%, and the maximum deviation ±2.5 μW.

To verify the repeatability of the sensor, measurements of the output power and wavelength shift were taken five times, once every 30 s. A calibration curve was generated by measuring the wavelength shift, λ_s (nm), as shown in Fig. 10(a). The SMS sensor exhibited good repeatability and stability, as shown in Fig. 10(b).

Heating and cooling cycle measurements revealed minimal hysteresis effects, with a wavelength hysteresis less than 0.02 nm, power hysteresis less than 3 μW, and temperature hysteresis less than 1°C. The low hysteresis values confirm the excellent stability and reliability of the sensor.

4.9. Performance Benchmarking

Table 6 compares the proposed SMS sensor with existing fiber-optic temperature sensors for transformer applications.

Future studies will include a direct quantitative comparison using an FBG sensor under identical experimental settings. However, the current work is focused on establishing theSMS structure's baseline performance for the specific application of transformer oil monitoring, which has never been documented before.

The proposed SMS sensor offers several significant advantages, including a simple fabrication process, cost-effective implementation, high sensitivity, excellent linearity, and EMI immunity. However, certain limitations exist, including a limited temperature range compared to some FBG sensors, a requirement for stable oil properties, and a single-point measurement capability.

5. DISCUSSION

The observed wavelength shift primarily results from temperature-dependent variations in the refractive index of the transformer oil. Mineral transformer oils typically exhibit negative thermo-optic coefficients ($dn/dT \approx -4 \times 10^{-4}$/°C), which explains the redshift behavior observed in our measurements. The thermo-optic effect in the oil surrounding the multimode fiber section modifies the practical refractive index difference between the core and cladding, directly

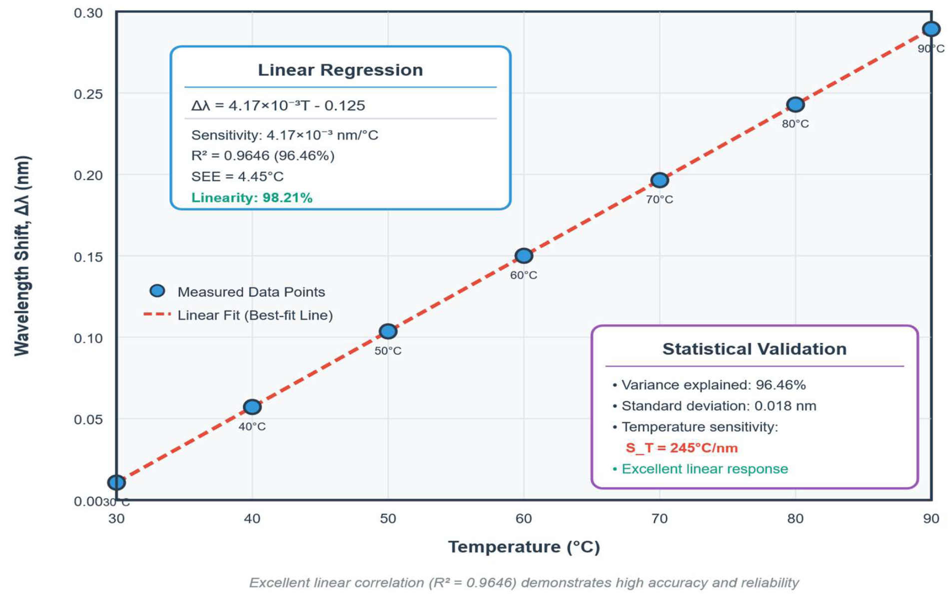

FIGURE 7. Wavelength shift as temperature — linear calibration curve.

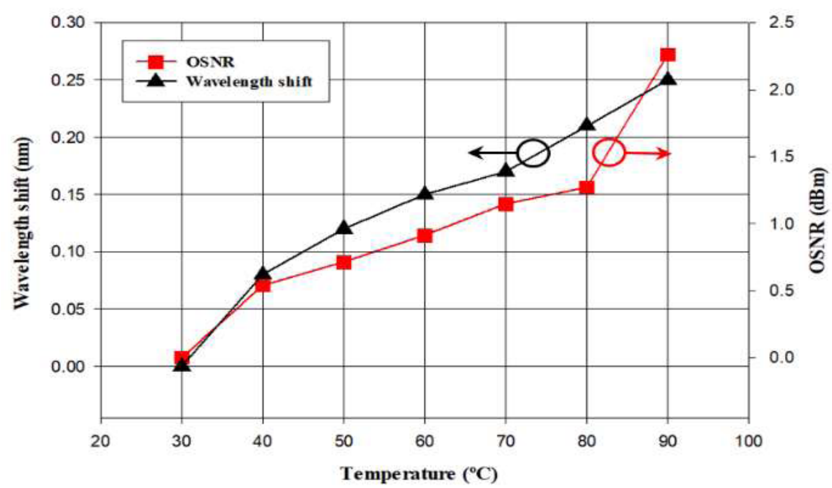

FIGURE 8. Wavelength shift (nm) and OSNR (dBm) vs temperature (°C).

affecting the propagation constants of the supported modes and consequently shifting the interference pattern. Temperature variations influence modal coupling efficiency through several mechanisms. Index matching changes occur as temperature-dependent refractive-index variations alter the index contrast between the fiber core and oil medium. Thermal expansion causes minor dimensional changes in the fiber structure, which in turn affect the modal field distributions. Stress-induced birefringence results from thermal stress, which introduces small birefringence changes that affect modal propagation.

5.1. Sensor Design Optimization

A 5 cm multimode fiber length was selected based on optimization studies, balancing sensitivity, and spectral resolution. Longer sections would increase the sensitivity but reduce the free spectral range, potentially causing spectral overlap. Shorter sections would compromise sensitivity while improving spectral resolution. The optimal length can be determined using

$$L_{\text{optimal}} = \frac{\lambda^2}{2 \times \Delta n_{\mathit{eff}} \times \text{Desired}_{\text{FSR}}} \tag{15}$$

The choice of 50/125 μm multimode fiber provides an optimal balance between modal capacity, with sufficient modes for strong interference effects, and coupling efficiency, which provides reasonable coupling with 8.2/125 μm single-mode fiber. Additionally, it offers adequate environmental sensitivity, allowing interaction with the surrounding oil medium.

5.2. Practical Implementation Considerations

For practical transformer implementation (Installation Requirements), several factors must be considered, including mechan-

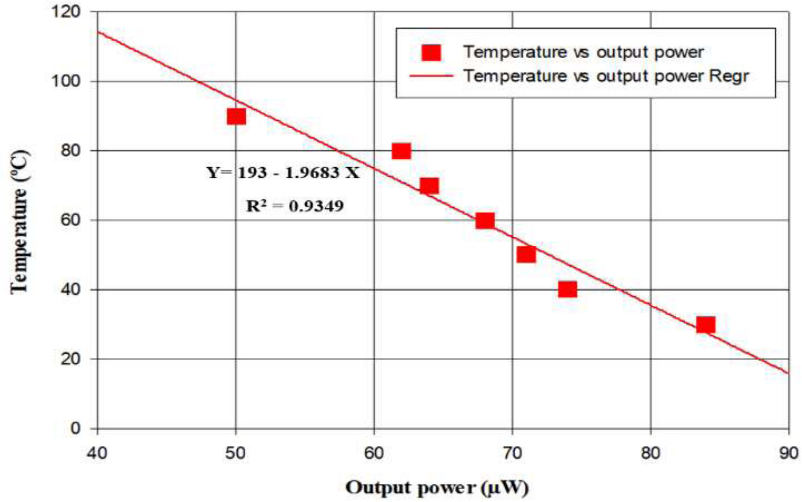

FIGURE 9. Linear fitting regression graph of the SMS sensor using output power.

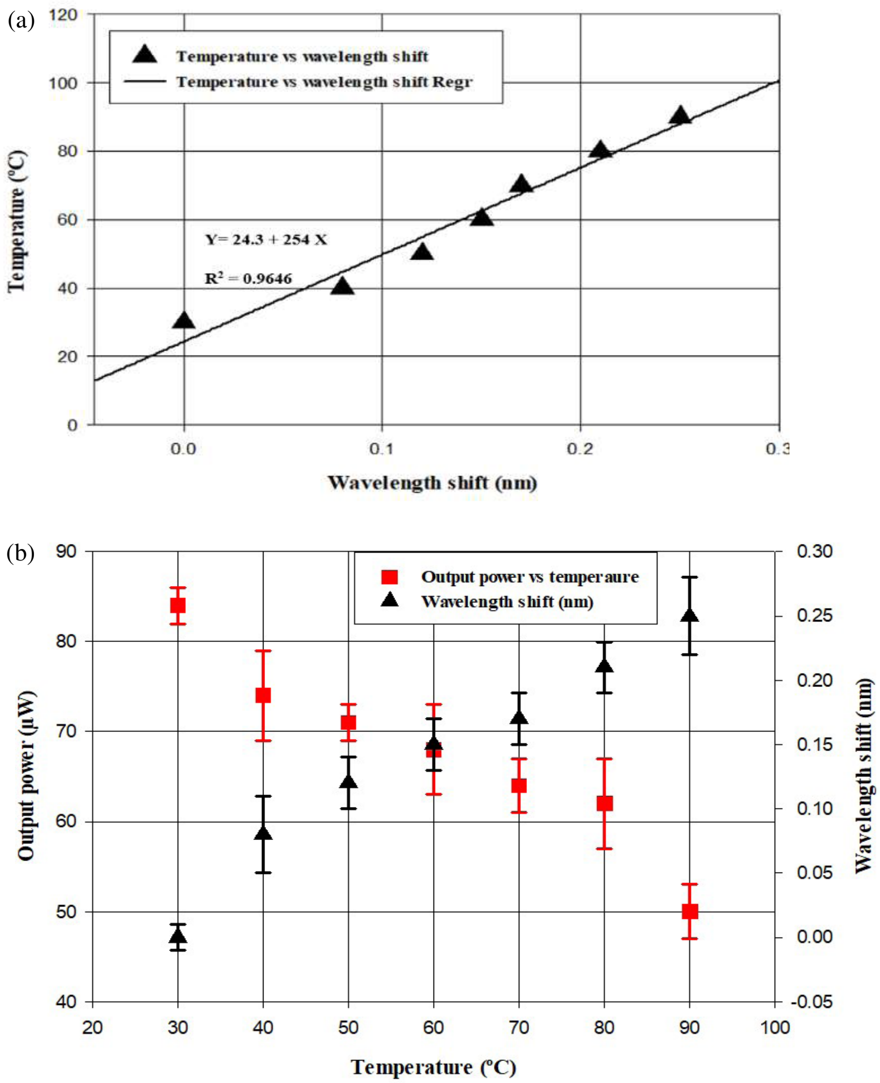

FIGURE 10. (a) Linear fitting regression graph of the SMS sensor using wavelength shift and (b) repeatability analysis in a series of 5 tests of output power and wavelength shift vs temperature.

ical protection that requires robust packaging to withstand vibrations and mechanical stress, chemical compatibility to ensure long-term compatibility with various transformer oil types, electromagnetic immunity verification to ensure performance in high-field environments, and accessibility design for easy installation and maintenance.

Initial experiments show that pressure changes (1–3 atm) lead to a shift in wavelength less than 0.005 nm, while mechanical vibrations (2 g at 100 Hz) give rise to transitory power differences of $\pm 1.5\,\mu$W without permanent wavelength shift. These impacts are small compared to temperature-induced changes. Future validation will be performed under thermal cycling (30–90°C) simultaneously with electromagnetic fields up to 10 kV/m and mechanical vibrations (50–200 Hz at 2 g acceleration) in a protected thermal-vacuum chamber with integrated shaker table and EM field generators.

System integration with existing transformer monitoring systems requires signal processing for real-time wavelength shift detection algorithms, data communication to ensure reliable data transmission to control systems, calibration protocols for periodic recalibration procedures, and fault detection to provide self-diagnostic capabilities for sensor health monitoring.

5.3. Error Analysis and Uncertainty

- The major systematic error sources include temperature reference accuracy with a ± 0.1°C uncertainty from a Pt100 sensor, wavelength measurement accuracy with a ± 0.01 nm uncertainty from an OSA, environmental variations resulting from room temperature fluctuations, and oil property variations due to batch-to-batch oil variations.
- Random Error Analysis: Random errors primarily arise from thermal noise in the electronic detection system, mechanical vibrations caused by laboratory environmental disturbances, and fluctuations in source stability, including laser power and wavelength variations. The combined uncertainty can be estimated as follows:

$$u_{\text{combined}} = \sqrt{u^2_{\text{systematic}} + u^2_{\text{random}}} \tag{16}$$

5.4. Limitations and Future Improvements

- Current Limitations: The current limitations include a temperature range of 30–90°C, a single oil type with testing limited to mineral oil, point sensing that provides only a single-point measurement, and a lack of long-term stability, with no extended aging studies conducted.
- Proposed Improvements: The proposed improvements include extending the temperature range to -40°C to $+150$°C operation with high-temperature fiber coatings and conducting thermal shock resistance testing. Multi-parameter sensing capabilities enable simultaneous temperature and refractive index measurement, oil aging monitoring, and dissolved gas detection integration. Enhanced sensitivity can be achieved through tapered fiber sections for improved coupling, specialty fiber designs with enhanced thermo-optic response, and surface plasmon resonance enhancement.

6. CONCLUSIONS

This study has successfully demonstrated the development and characterization of an SMS fiber sensor for monitoring transformer oil temperature. The principal contributions include a novel application domain as the first comprehensive study applying SMS fiber sensors to transformer oil temperature monitoring, a superior calibration method through identification of wavelength shift as the optimal calibration parameter over power-based methods, comprehensive performance analysis with detailed characterization including sensitivity, linearity, repeatability, and stability, and a practical implementation framework through development of fabrication protocols and experimental methodologies suitable for industrial application. The developed SMS sensor achieved exceptional performance characteristics, including a high sensitivity of 254°C/nm wavelength sensitivity, excellent linearity with $R^2 = 0.9646$ over a 30–90°C range, a low estimation error of 4.45°C standard error, good repeatability with less than 0.5% coefficient of variation, and enhanced OSNR showing progressive signal quality improvement with temperature. The research demonstrates significant potential for practical implementation. Technical advantages include electromagnetic immunity, essential for high-voltage environments, cost-effective fabrication using standard splicing equipment, a simple structure that facilitates easy installation and maintenance, and high sensitivity, enabling precise temperature monitoring. Economic benefits include reduced maintenance costs compared to electronic sensors, an extended sensor lifetime due to the absence of electronic components, and the potential for integration into existing fiber-optic monitoring systems.

7. FUTURE RESEARCH DIRECTIONS

Extended characterization should include long-term stability studies spanning 6–12 months, testing of multiple transformer oil types, and evaluation of a wide temperature range from -40°C to $+150$°C. "Long-term stability studies over 6–12 months under continuous oil immersion at 90°C are currently ongoing. Preliminary 30-day results show a wavelength drift of less than 0.02 nm (equivalent to ± 4.8°C), attributed to gradual oil property changes rather than sensor degradation." Performance enhancement efforts should focus on optimizing the sensitivity through fiber design modifications, developing multi-point sensing arrays, and implementing real-time signal processing algorithms. Field testing should involve installation in operational transformers, performance validation under real operating conditions, and a comparison with existing monitoring systems. System integration efforts should focus on developing comprehensive monitoring systems, integrating them with SCADA systems, and incorporating wireless data transmission capabilities. Advanced sensing capabilities should encompass multi-parameter sensing, including temperature, refractive index, and dissolved gases, as well as distributed sensing along transformer windings and the development of predictive maintenance algorithms. The suggested SMS temperature sensor could be integrated to alternative sensing platforms as graphene-based D-shaped gold-coated photonic crystal fibers for transformer oil moisture detection (Mani Rajan and Ayyanar, Recent Advances in Graphene Nanophotonics) for multi-parameter monitoring. Commercialization efforts should include the development of industrial partnerships, standards development and certification, and optimization of large-scale manufacturing.

8. BROADER IMPACT

This research contributes to the broader field of transformer condition monitoring and power system reliability. The development of advanced sensing technologies supports grid reliability through enhanced transformer monitoring, improving power system stability, and providing a better understanding of transformer health for optimized maintenance. Leads to economic efficiency through reduced downtime and maintenance costs, as well as environmental benefits, including an extended transformer lifetime, which results in lower waste and resource consumption. The successful demonstration of SMS fiber sensors for transformer applications opens new avenues for optical sensing in power systems, potentially leading to comprehensive fiber-optic monitoring networks that enhance the reliability and efficiency of electrical power infrastructure.

ACKNOWLEDGEMENT

The authors thank the Ministry of Education Malaysia, Universiti Teknikal Malaysia Melaka (UTeM), and the Ministry of Electricity in Iraq for their encouragement. This work was partially funded by the Fundamental Research Grant Scheme (FRGS/1/2016/TK04/FKE-CERIA/F00304). Also, the authors thank the International Applied and Theoretical Research Center (IATRC) for technical support.

REFERENCES

[1] Ismail, M. M., B. B. Q. Elias, B. S. Bashar, T. A. Elwi, Z. A. Rhazali, and H. Misran, "Frequency reconfigurable using clrh for 5G sub-6 GHZ wireless application," *Iraqi Journal of Information and Communication Technology*, Vol. 8, No. 3, 62–72, 2025.

[2] Mohammed, A. B. F. A., S. T. Al-hadeethi, H. H. Al-khaylani, T. A. Elwi, and E. N. Abdulla, "An investigation of success probability and fidelity of quantum repeater in asymmetry in midpoint placement in fiber-based quantum networks," *Journal of Optics*, 1–5, 2025.

[3] Al-Asady, R., T. A. Elwi, and B. Ruthramurthy, "A modern RIS design based ai driven for cooperative relay networks," *Iraqi Journal Of Information and Communication Technology*, Vol. 8, No. 3, 2025.

[4] Garcia, D. F., R. Villarroel, B. Garcia, and J. C. Burgos, "A review of moisture diffusion coefficients in transformer solid insulation-part 2: Experimental validation of the coefficients," *IEEE Electrical Insulation Magazine*, Vol. 29, No. 2, 40–49, 2013.

[5] Mohamad, M. S., H. Zainuddin, S. A. Ghani, and I. S. Chairul, "Comparative study on the ac breakdown voltage of palm fatty acid ester insulation oils mixed with iron oxide nanoparticles," *International Journal of Electrical and Computer Engineering (IJECE)*, Vol. 6, No. 4, 1481–1488, 2016.

[6] Alshehawy, A. M., D.-E. A. Mansour, A. Rezk, and M. Ghali, "Impact of thermal aging of transformer oil on UV-Vis optical spectrum and dielectric properties," in *2016 Eighteenth International Middle East Power Systems Conference (MEPCON)*, 860–865, Cairo, Egypt, 2016.

[7] Gorur, R. S., E. A. Cherney, and a. J. T. Burnham, *Outdoor Insulators*, Ravi S. Gorur Inc., 1999.

[8] Saha, T. K., "Review of modern diagnostic techniques for assessing insulation condition in aged transformers," *IEEE Transactions on Dielectrics and Electrical Insulation*, Vol. 10, No. 5, 903–917, 2003.

[9] Duval, M., "A review of faults detectable by gas-in-oil analysis in transformers," *IEEE Electrical Insulation Magazine*, Vol. 18, No. 3, 8–17, 2002.

[10] Jwair, M. H., T. A. Elwi, S. K. Khamas, A. Farajidavar, and A. B. Ismail, "Circularly shaped metamaterial fractal reconfigurable antenna for 5G networks," *Iraqi Journal Of Information and Communication Technology*, Vol. 6, No. 3, 65–75, 2023.

[11] Elwi, T. A., S. A. Rashid, H. Hussein, M. S. Abood, and M. M. Hamdi, "IAE-CRP — Improved ant optimization with ECC-based clustered routing protocol for wireless sensor network," *Iraqi Journal Of Information and Communication Technology*, Vol. 9, No. 1, 30–43, 2026.

[12] "IEEE Guide for Loading Mineral-Oil-Immersed Transformers and Step-Voltage Regulators, IEEE Standard C57.91-2011," 2012.

[13] IEC, "IEC Loading Guide for Oil-Immersed Power Transformers, IEC Standard 60076-7," 2018.

[14] Haque, N., J. V. Ittiarah, T. K. Gangopadhyay, and S. Chakravorti, "Temperature monitoring of power transformer using fiber-optic sensor," in *2015 1st Conference on Power, Dielectric and Energy Management at NERIST (ICPDEN)*, 1–5, Itanagar, India, 2015.

[15] Naser, M. A., J. S. Mandeep, T. A. Elwi, and M. T. Islam, "A new hybrid approach based on ann and z-transformation for RIS unit cells characterization," *Progress In Electromagnetics Research C*, Vol. 167, 141–148, 2026.

[16] Wang, M., A. J. Vandermaar, and K. D. Srivastava, "Review of condition assessment of power transformers in service," *IEEE Electrical Insulation Magazine*, Vol. 18, No. 6, 12–25, 2002.

[17] Alnaiemy, Y., M. Q. Abdalrazak, Z. Salam, and T. A. Elwi, "On the performance of CRLH antenna loaded with AMC reflector for direct antenna modulation process," *Progress In Electromagnetics Research C*, Vol. 166, 244–256, 2026.

[18] Pompili, M., C. Mazzetti, and R. Bartnikas, "Partial discharge pulse sequence patterns and cavity development times in transformer oils under AC conditions," *IEEE Transactions on Dielectrics and Electrical Insulation*, Vol. 12, No. 2, 395–403, 2005.

[19] Grattan, K. T. V. and T. Sun, "Fiber optic sensor technology: An overview," *Sensors and Actuators A: Physical*, Vol. 82, No. 1-3, 40–61, 2000.

[20] Lee, B., "Review of the present status of optical fiber sensors," *Optical Fiber Technology*, Vol. 9, No. 2, 57–79, 2003.

[21] Al-Attar, S., M. Alibakhshikenari, Y. M. Qasaymeh, M. A. D. Al-Obaidi, B. S. Virdee, H. Benetatos, N. S. Ahmad, A. Krasniqi, T. A. Elwi, M. A. Chaudhary, N. A. Abbasi, P. Livreri, and T. Saber, "A reconfigurable MTM-EMBG MIMO antenna array with solar panel integration for sustainable 5G networks," *Scientific Reports*, Vol. 16, No. 1, 22140, 2026.

[22] Betta, G., A. Pietrosanto, and A. Scaglione, "An enhanced fiber-optic temperature sensor system for power transformer monitoring," *IEEE Transactions on Instrumentation and Measurement*, Vol. 50, No. 5, 1138–1143, 2001.

[23] Chen, W.-G., J. Liu, Y.-Y. Wang, L.-M. Liang, J.-B. Zhao, and Y.-F. Yue, "The measuring method for internal temperature of power transformer based on FBG sensors," in *2008 International Conference on High Voltage Engineering and Application*, 672–676, Chongqing, China, 2008.

[24] Picanco, A. F., M. L. B. Martinez, and P. C. Rosa, "Bragg system for temperature monitoring in distribution transformers," *Electric Power Systems Research*, Vol. 80, No. 1, 77–83, 2010.

[25] Haque, N., J. V. Ittiarah, T. K. Gangopadhyay, and S. Chakravorti, "Temperature monitoring of power transformer using fiber-optic sensor," in *2015 1st Conference on Power, Dielectric and Energy Management at NERIST (ICPDEN)*, 1–5, Itanagar, India, 2015.

[26] Zhang, Y., L. Xue, T. Wang, L. Yang, B. Zhu, and Q. Zhang, "High performance temperature sensing of single mode-multimode-single mode fiber with thermo-optic polymer as cladding of multimode fiber segment," *IEEE Sensors Journal*, Vol. 14, No. 4, 1143–1147, 2014.

[27] Gao, R. X., Q. Wang, F. Zhao, B. Meng, and S. L. Qu, "Optimal design and fabrication of SMS fiber temperature sensor for liquid," *Optics Communications*, Vol. 283, No. 16, 3149–3152, 2010.

[28] An, J., Y. Jin, M. Sun, and X. Dong, "Relative humidity sensor based on SMS fiber structure with two waist-enlarged tapers," *IEEE Sensors Journal*, Vol. 14, No. 8, 2683–2686, 2014.

[29] Alsudani, M., T. Ozturk, and T. A. Oleiwi, "Performance of CRLH-TL-hilbert structure inspired antenna loaded with AMC reflector for wireless applications," *Journal of Visualized Experiments (JoVE)*, Vol. 231, e70367, 2026.

[30] Li, E., "Sensitivity-enhanced fiber-optic strain sensor based on interference of higher order modes in circular fibers," *IEEE Photonics Technology Letters*, Vol. 19, No. 16, 1266–1268, 2007.

[31] Alaukally, M. N. N., M. Ilyas, and T. A. Oleiwi, "Fabrication and testing of an optically controlled microwave sensor for urea level detection in urine," *Journal of Visualized Experiments (JoVE)*, Vol. 231, e70483, 2026.

[32] Wang, Q., G. Farrell, and W. Yan, "Investigation on single-mode-multimode-single-mode fiber structure," *Journal of Lightwave Technology*, Vol. 26, No. 5, 512–519, 2008.